Integration of Waveguide-Type Wavelength Demultiplexing Photodetectors by the Selective Intermixing of an InGaAs–InGaAsP Quantum-Well Structure

Deok Ho Yeo, Kyung H. Yoon, Hang Ro Kim, and Sung June Kim, *Member, IEEE*

***Abstract*—Using the selective intermixing of an InGaAs–InGaAsP multiquantum-well (MQW) structure, a wavelength demultiplexing photodetector which can demultiplex two widely separated wavelengths was fabricated. An InGaAs–InGaAsP MQW with a u-InP cladding layer and a u-InGaAs cap layer, grown by metal organic chemical vapor deposition was used. Selective area intermixing of the InGaAs–InGaAsP MQW structure was done by a rapid thermal annealing after the deposition and patterning of the SiO_2 dielectric layer on the InGaAs cap layer. The integrated structure consists of shorter and longer wavelength sections, separated by an absorber section. Shorter wavelength and absorber sections were intermixed with the SiO_2 dielectric layer. At a wavelength of 1477 nm, the output photocurrent ratio was enhanced as the length of the absorber region increased and a ratio of over 30 dB was observed, while at a wavelength of 1561 nm, an output photocurrent ratio of 18.9 dB was observed.**

***Index Terms*—Dielectric cap annealing, dual wavelength photodetector, InGaAs–InGaAsP multiquantum wells, integrated optics, quantum-well intermixing, waveguide photodetector, wavelength demultiplexing.**

I. Introduction

DUE TO the current development of fiber manufacturing technologies and rare earth-doped fiber amplifiers, wide wavelength ranges (S, S^+, C, L band), which were difficult to utilize in the past, now hold great promise for future applications [1]–[2]. Thus, photodetectors (PDs) that can demultiplex wavelength bands have a great deal of potential relative to fiber-optic communication systems of the future. In achieving such devices that are monolithic, techniques for fabricating regions that have different bandgap energies on the same wafer are required. Several techniques exist for fabricating such regions selectively: selective area growth using SiO_2 masks in conjunction with metal organic chemical vapor deposition (MOCVD) [3], laser-assisted metal organic molecular beam epitaxy (MOMBE) [4], the quantum-confined Stark effect (QCSE) in multiquantum-well (MQW) structures [5], and quantum-well intermixing techniques [6]. Among these, the intermixing of MQW structures is a simple and useful technique for the fabrication of optoelectronic devices requiring different bandgap energies on a chip. This technique permits postgrowth modification to the bandgap energy of the MQW, thus providing a flexible, simple and low cost process compared to selective area epitaxy or selective etching and regrowth [6]–[12]. The intermixing techniques for InP-based MQW's are important because of their potential application in 1.55 μm fiber-optic communication systems in optoelectronic devices which require different bandgap energies. We recently reported on an impurity free vacancy diffusion (IFVD) technique using an SiO_2 dielectric film on an InGaAs cap layer for promoting the intermixing of an InGaAs–InP MQW system, in which large bandgap shifts were observed [7]. This method was also applied to InGaAsP–InP and InGaAs–InGaAsP MQW systems where the spatial resolution of the IFVD process was found to be less than 3 μm and a large loss reduction in ridge-type waveguides was investigated [8], [9]. For the compressively strained InGaAs–InGaAsP quantum-well structure, a large bandgap shift was obtained at a relatively low annealing temperature compared to lattice matched MQW structure [10].

In this work, this technique is extended to the fabrication of waveguide type photodetectors that can demultiplex *two widely separated wavelengths* capable of separating widely separated wavelengths, not for wavelength division multiplexing (WDM) and dense WDM (DWDM). Our work is focused on the fabrication of a demultiplexing photodetector which can operate in the 1.48-/1.55-μm wavelength ranges by intermixing of the InGaAs–InGaAsP MQW structure by the SiO_2 dielectric cap annealing process. Section II describes the fabrication process, while Section III examines the spectral responses and demultiplexing functions of the fabricated devices. However, this type of photodetector is not adequate for application in WDM and DWDM systems.

II. Experimental Methods and Device Fabrication

An InGaAs–InGaAsP MQW grown by metal organic chemical vapor deposition (MOCVD) was used for this experiment. The epitaxial layer structure was grown on an n-InP (S-doped; $1 \times 10^{18}\text{cm}^{-3}$) substrate and included a 1-μm S-doped n-InP buffer, a 0.15-μm u-$In_{0.85}Ga_{0.15}As_{0.3}P_{0.7}$ layer, a 0.05-μm u-$In_{0.81}Ga_{0.19}As_{0.43}P_{0.57}$ confinement layer on both sides of the MQW, a 0.5-μm u-InP cladding layer, and a 0.1-μm

Manuscript received August 15, 2000; revised February 26, 2001. This work was supported in part by the Korea Telecommunication Corporation and by the Ministry of Education, Korea, under the Brain Korea 2000 Project.

The authors are with the School of Electrical Engineering, Seoul National University, Seoul, Korea (e-mail: kim@helios.snu.ac.kr).

Publisher Item Identifier S 0018-9197(01)04298-1.

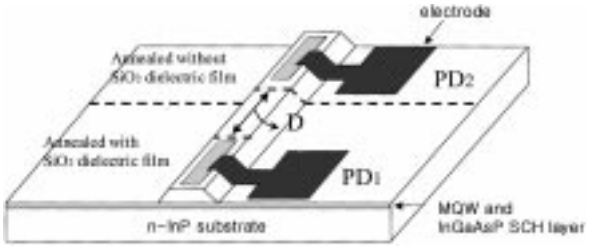

Fig. 1. Schematic diagram of integrated waveguide type photodetectors. The large bandgap area was annealed with an SiO_2 dielectric layer on an InGaAs cap layer and the small bandgap area was annealed without the SiO_2 dielectric layer.

u-$In_{0.53}Ga_{0.47}$ As cap layer. The MQW structure consists of five layers of 84-Å $In_{0.53}Ga_{0.47}As$ and four layers of 100 Å $In_{0.77}Ga_{0.23}As_{0.47}P_{0.53}$. The epitaxial layers were intentionally undoped, in order to avoid impurity-induced disordering by Zn diffusion during the intermixing process and electrical isolation between devices [12]. A schematic diagram of the integrated waveguide type photodetectors is shown in Fig. 1. Regions for shorter wavelength detection, a dummy waveguide as an absorber region, and a longer wavelength are linearly lined up and coupled light propagates each region through a rib waveguide. The width of the waveguide is 20 μm, the length of each detector is 250 μm, and that of the absorber region varies from 100 to 900 μm. For the as-grown epitaxial layer, the PL peak wavelength of the MQW was found to be 1480 nm at 10 K and 1588 nm at room temperature. A 1700 Å SiO_2 dielectric layer was deposited on the InGaAs cap layer by plasma-enhanced chemical vapor deposition (PECVD) to enhance the intermixing of the MQW. An SiO_2 dielectric layer was patterned using photolithography and a wet chemical etch was achieved using buffered HF. The sample was annealed at 750 °C, for 45 s. Regions for shorter wavelength detection and the dummy waveguide were annealed with a SiO_2 dielectric layer and the longer wavelength region was annealed without it. Regions with and without the SiO_2 dielectric layer had bandgap shifts of 26 and 79 meV, respectively, and sufficient bandgap difference was achieved. An MQW annealed without the SiO_2 dielectric layer shows a slight increase in bandgap compared with the as-grown MQW. This is due to the self-diffusion of the well and barrier materials at the high annealing temperature employed. The origins of the PL peak shift in the integrated region are considered to be well and barrier composition intermixing. Secondary ion mass spectroscopy (SIMS) of In, Ga, As, P, and S before and after the annealing process were investigated. From the measurements, it was found that interdiffusion of both groups III and V elements took place in the MQW and S did not diffuse significantly at the interface of the u-InGaAsP confinement and n-InP buffer layer, in contrast to Zn at a high annealing temperature [8], [12].

After annealing, the SiO_2 dielectric layer was removed by wet chemical etching. The InGaAs cap layer between the two detectors was wet-chemically removed to reduce propagation loss. A P-ohmic layer was formed at the contact region by Zn_3P_2 evaporation and annealing so that two photodetectors could be isolated electrically. The rib waveguide was formed by wet etching and the SiO_2 dielectric layer was deposited by PECVD for the passivation layer. Au–AuZn–Cr–Au and AuGe–Ni–Au multilevel systems were used for p- and n-type contact metal. The amount of the isolated resistance between the two photodiodes was about 10 kΩ for the 100-μm absorber region and increased as the absorber region length increased. This value was comparable to other reported experimental results without an electrical ground for the absorber region [4]. Thus, selective area Zn-doping for p-type layer formation and electrical isolation of the photodetectors by separation is simple and effective when this approach is used.

III. Results and Discussion

The spectral response of the photodetector was characterized using a tunable laser. Two tunable lasers were used to obtain a wide spectral range and, as a result, a wavelength range from 1480 to 1625 nm was obtained. Light was end-fiber coupled to the photodetector using lensed fiber with spot size of 3 μm. The input polarization was set to the transverse electric (TE) or transverse magnetic (TM) mode by means of a polarization controller.

The coupling efficiency γ was calculated by integration over the area of overlap between the normalized optical field of the light emitted from the lensed fiber $\Psi(x, y) = \psi_x(x)\psi_y(y)$, and the normalized optical field of the guided lightwave through the waveguide $\Phi_{ij}(x, y) = \phi_{xi}(x)\phi_{yj}(y)$

$$\gamma = \frac{\sum_{i,j} \left| \iint \Psi(x, y)\Phi_{i,j}(x, y)\, dx\, dy \right|^2}{\left| \iint \Psi(x, y)\, dx\, dy \right|^2} \cong \sum_j \left| \int \psi_y(y)\phi_{y,j}(y)\, dy \right|^2 \quad (1)$$

where i and j are the orders in the x and y directions of the guided light mode at the waveguide, respectively. Equation (1) is approximate because the width of the waveguide is much wider than the distribution of $\psi_x(x)$.

The photocurrent generated in the waveguide can be written as

$$I = \left(\frac{e\lambda}{hc}\right) P_0 \gamma (1 - R)\eta \frac{\Gamma \alpha^{\text{int}}(\lambda)}{\alpha(\lambda)} \left(1 - e^{-\alpha(\lambda)L}\right) \quad (2)$$

where

$e\lambda/hc$	conversion factor from optical power to photocurrent;
P_0	input optical;
R	reflectance at the waveguide facet;
η	internal quantum efficiency;
Γ	optical confinement factor of the active layer;
$\alpha^{\text{int}}(\lambda)$	interband absorption coefficient;

and $\alpha(\lambda) = \Gamma\alpha^{\text{int}}(\lambda)_+\alpha_0$ is the total attenuation coefficient, where α_0 represents the scattering loss coefficient of the waveguide and L is the length of the waveguide.

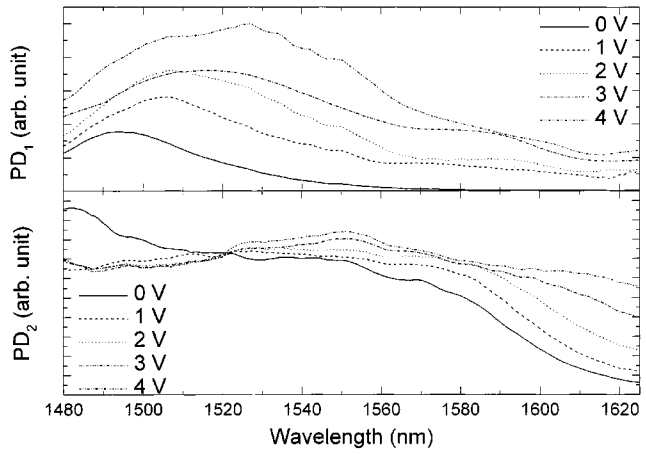

(a)

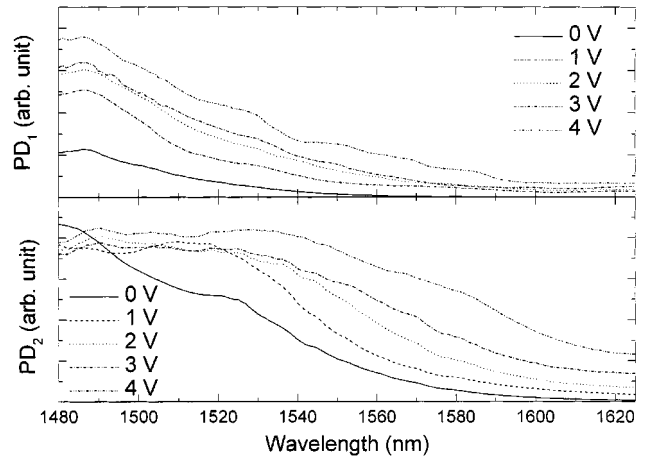

(b)

Fig. 2. Photocurrent spectra of individual photodetectors as a function of applied bias voltage. Red shifts of photocurrent spectra due to QCSE are seen for the: (a) TE and (b) TM mode.

Fig. 2 shows the measured photocurrent spectrum of an individual photodetector as a function of applied reverse bias for the polarization of the TE/TM modes, respectively. The photocurrent was slightly reduced near 1480 nm due to the instability of the tunable laser light source. A photocurrent spectrum of PD_1 with a larger bandgap energy shows a blue shift with respect to that of PD_2 for smaller bandgap energy, as would be expected from PL measurements. As shown in the figure, red shifts of photocurrent were observed due to the QCSE when the reverse bias was applied to the photodetector. The responsivities of each unit devices at zero bias are summarized in Table I for two wavelengths of 1477 and 1561 nm. The light source was a distributed feedback (DFB) laser diode. The theoretical limit of responsivity was calculated by assuming that the length of the waveguide was infinite. If the input waveguide facet was anti-reflection coated, the responsivity of the photodetectors would be enhanced more.

The wavelength demultiplexing function of the integrated photodetectors was also measured. The spectral response was measured at zero bias, because, when the reverse bias was applied to the photodetector, the photocurrent ratio between PD_1 and PD_2 became worse due to a red shift in the photocurrent spectrum.

For a multisegment waveguide photodetector, the photocurrent generated in segment i, of length Li, can be expressed as [5]

$$Ii = \left(\frac{e\lambda}{hc}\right) P_0\gamma(1-R)\eta\frac{\Gamma\alpha_i^{\text{int}}(\lambda)}{\alpha_i(\lambda)} \cdot \exp\left(-\sum_{k=1}^{i-1}\alpha_k(\lambda)L_k\right)\left(1-e^{-\alpha_i(\lambda)L_i}\right) \quad (3)$$

where i denotes a segment of the waveguide type photodetector.

From (3), light coupled to PD_1 propagates through the waveguide and its intensity decreases due to absorption and propagation loss in the MQW. Non-absorbed light at PD_1 and the absorber region propagates to PD_2, thus generating photocurrent. Fig. 3 shows a normalized photocurrent spectrum of integrated wavelength demultiplexing photodetectors for the TE and TM modes, respectively. The generated photocurrent spectrum of PD_1 will be the same as shown in Fig. 2 but that of PD_2 will be deformed. As can be seen in (3), the amount of photons reaching the PD_2 region decreases, as the result of absorption and scattering in the previous region. Therefore, the photocurrent of PD_2 at short wavelength was greatly decreased. The photocurrent of PD_1 was reduced to nearly zero at wavelengths over 1570 nm and the peak of the photocurrent in the spectral response of PD_2 was near 1570 nm. As can be seen in Fig. 3, it is clear that the fabricated photodetectors can demultiplex wavelengths of 1480 and 1550 nm.

Crosstalk of the photodetectors (PD1 and PD2) can be defined by

$$C = 10 \times \log\left(\frac{\text{PD}_2}{\text{PD}_1}\right) \quad (4)$$

when the light with short wavelength is coupled, and by

$$C = 10 \times \log\left(\frac{\text{PD}_1}{\text{PD}_2}\right) \quad (5)$$

when the long wavelength light is coupled to the waveguide. So, the crosstalk can be viewed completely by plotting the photocurrent ratio of PD_2 and PD_1 (PD_2/PD_1).

The crosstalk for the TE and TM mode light at short wavelength is due to incomplete absorption at PD_1. This is also the result for scattered and unguided light that reaches PD_2 and the generated photocurrent. By increasing the spacing between the two photodetectors, this crosstalk can be further reduced. Fig. 4 shows changes in the photocurrent ratio at 1477 and 1561 nm as a function of the spacing between photodetectors. Light from a single-mode DFB laser diode was coupled to the wavelength demultiplexing photodetectors and the photocurrent ratios of PD_1 and PD_2 were measured as a function of the absorber region length.

As would be expected from (3), the photocurrent and responsivity of PD_2 will be decreased as will the ratio of PD_2 to PD_1. A change in the photocurrent ratio at 1477 nm clearly shows the effect of the absorber region. An increase in spacing between the two devices resulted in an enhancement in the photocurrent ratio by reducing the responsivity of PD_2. The responsivity of PD_2 for the TE mode was reduced from 18 mA/W to 73 μA/W

TABLE I
RESPONSIVITY OF UNIT DEVICES (PD_1 AND PD_2) AT ZERO BIAS FOR TWO WAVELENGTHS (1477 AND 1561 NM). LIGHT WAS END-FACET COUPLED TO EACH UNIT DEVICE USING LENSED FIBER. THEORETICAL LIMITS WERE CALCULATED ASSUMING THAT LIGHT IS FULLY ABSORBED AT THE WAVEGUIDE PHOTODETECTORS

	PD_1 (TE/TM)	PD_2 (TE/TM)	Theoretical limit: TE/TM (A/W)
1477 nm	0.073/0.08 A/W	0.115/0.123 A/W	0.2739/0.2717
1561 nm	368/97 μA/W	0.1/0.08 A/W	0.3042/0.3019

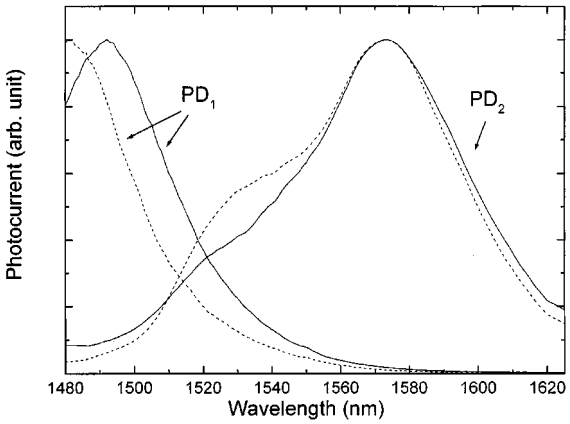

Fig. 3. Normalized photocurrent spectra of integrated waveguide photodetectors for TE (solid) and TM (dot) mode.

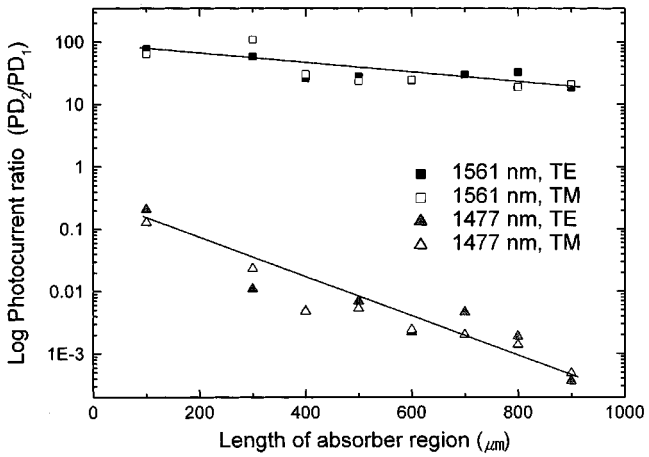

Fig. 4. Photocurrent ratio of PD_1 and PD_2 when the wavelength of coupled light was 1477 nm (triangle) and 1561 (square) nm. TE and TM modes are presented as solid and open symbols, respectively.

by increasing the length of the absorber from 100 to 900 μm and, hence, the crosstalk (PD_1/PD_2) was changed from 6 to 30 dB.

For the wavelength of 1561 nm, the responsivity of the PD_2 for the TE mode was reduced from 28 to 6.6 mA/W by increasing the length of the absorber from 100 to 900 μm and, hence, the crosstalk of PD_2 and PD_1 (PD_2/PD_1) was changed from 18.9 to 12.6 dB. Reduced responsivity is caused by absorption and waveguide loss of the injected beam while propagating to PD_2. The reduction in the photocurrent ratio as a function of absorber region are 78 dB/cm ($a = 18$/cm) and 304 dB/cm ($a = 70$/cm) at wavelengths of 1561 and 1477 nm, respectively.

As a result, it is necessary to compromise the length of the absorber region to fit the system requirements. Larsson *et al.* fabricated and measured the characteristics of tunable GaAs–AlGaAs superlattice p-i-n photodetectors [16]. The absorption spectrum was tuned using the QCSE by applying external reverse bias to the photodetectors. They measured the bit-error rate (BER) at a data rate of 100 Mb/s for the various crosstalks. Based on the measurement, a crosstalk of 10 dB is sufficient to achieve a BER less than 10^{-9}. Thus, it can be safely said from Fig. 4 that for the demultiplexing of 1477- and 1561-nm wavelengths using the fabricated device, 300 μm of the absorption region is sufficient for system applications. If the devices were operated at reverse bias, crosstalk between two photodetectors would be degraded. For the wavelength of 1561 nm, the photocurrent ratio of PD_2 and PD_1 (PD_2/PD_1) will be degraded as much as 1/30 because of when the reverse bias changes from 0 to -4 V. This is because the photocurrent spectrum of the photodetector shows red shifts due to the QCSE when the reverse bias is applied. Thus, zero bias was applied to the devices for sufficient crosstalk.

Optimizing the epitaxial layer structure and intermixing conditions can further improve the performance of the fabricated device with respect to crosstalk, responsivity and speed. This is especially so when the bandgap difference of the two areas (PD_1, PD_2) after the annealing process is large. In this case, absorption loss and photocurrent generation for 1561 nm is small in the area annealed with the SiO_2 dielectric cap and low crosstalk is expected in this wavelength. In order to achieve a large bandgap difference, an MQW with a large bandgap difference, such as InGaAs(P)–InP or InGaAs–InAlAs, is preferable because under the same annealing condition, a larger bandgap shift can be obtained compared with lattice matched InGaAs–InGaAsP MQW structure [7]–[9]. This is because confined electron, heavy and light hole energies in the MQW will be affected to a greater extent and bandgap shifts for a fully intermixed MQW will be larger for thinner wells and larger bandgap difference between well and barrier materials. Although bandgap shifts for tensile-strained MQWs which

had been annealed with an SiO_2 dielectric cap is very large under relatively low annealing temperatures, it cannot be used because bandgap shifts without the SiO_2 dielectric are also large, since self-interdiffusion of materials in the MQW is large and the thickness of wells is small [10]. For high-speed optical communications, the capacitance of the photodetector should be below 30 fF, but the calculated capacitance of the fabricated device is about 1 pF and thus the device size must be reduced [13], [14]. To accomplish this, an increase in the number of quantum wells and an enlarged InGaAsP SCH layer is needed so that the waveguide is in multimode operation. The increased number of quantum wells will enlarge the total absorption coefficients and the length of the photodetector can be reduced for fixed quantum efficiency and responsivity. Multimode operation will result in a larger coupling efficiency and it also helps to reduce the device size and the capacitance [13]. However, the number of quantum wells is limited because the interdiffusion coefficients of MQW will decrease as the depth of quantum wells from the surface of the wafer and the bandgap is broadened in the area annealed with the SiO_2 dielectric layer [15]. Thus, it is also necessary to optimize the epitaxial layer structure to have low crosstalk, small device size and good coupling efficiency and to satisfy the system requirements.

IV. Conclusion

A simple and effective fabrication method for producing a two wavelength demultiplexing p-i-n waveguide type photodetector was successfully demonstrated using selective area intermixing of an InGaAs–InGaAsP MQW structure by SiO_2 dielectric cap annealing. A photodetector with a large bandgap shows a blue shift in the photocurrent spectrum for the TE and TM mode with respect to that of small bandgap. It was shown that integrated photodetectors can demultiplex wavelengths of 1477 and 1561 nm. The photocurrent ratio was greatly enhanced by increasing the length of the absorber region between the two photodetectors. This area-selective quantum-well intermixing can be further applied in the implementation of the monolithic integration of optical devices on a chip.

Acknowledgment

The authors would like to thank S. G. Lee and S. I. Kim at Korea Telecommunication Corporation for their helpful advice. The authors are also grateful to I. S. Choi for his assistance in fabricating the devices that were used in the study.

References

[1] T. Komukai, T. Yamamoto, T. Sugawa, and Y. Miyajima, "Upconversion pumped thulium-doped fluoride fiber amplifier and laser operating at 1.47 μm," *IEEE J. Quantum Electron.*, vol. 31, pp. 1880–1889, 1995.

[2] Y. Nishida, M. Yamada, T. Kanamori, K. Kobayashi, J. Temmyo, S. Sudo, and Y. Ohishi, "Development of an efficient praseodymium-doped fiber amplifier," *IEEE J. Quantum Electron.*, vol. 34, pp. 1332–1339, 1998.

[3] M. Aoki, M. Suzuki, H. Sano, T. Kawano, T. Ido, T. Taniwatari, K. Uomi, and A. Taki, "InGaAs/InGaAsP MQW electroabsorption modulator integrated with a DFB laser fabricated by bandgap energy control selective area MOCVD," *IEEE J. Quantum Electron.*, vol. 27, pp. 2088–2096, 1993.

[4] Y. Suzuki, R. Iga, T. Yamada, H. Sugiur, and M. Naganuma, "Crosstalk characteristics of a 1.3-μm/1.5-μm wavelength demultiplexing photodetector using laser-assisted MOMBE growth," *J. Lightwave Technol.*, vol. 17, pp. 483–489, 1999.

[5] D. Moss, F. Ye, D. Landheer, P. E. Jessop, J. G. Simmons, H. G. Champion, I. Templeton, and F. Chatenooud, "Ridge waveguide quantum-well wavelength division demultiplexing detector with four channels," *IEEE Photon. Technol. Lett.*, vol. 4, pp. 756–759, July 1992.

[6] A. N. M. Masum Choudhury, P. Melman, A. Silletti, Emil. S. Koteles, B. Foley, and B. Elman, "Metal–semiconductor–metal demultiplexing waveguide photodetectors in InGaAs/GaAs quantum well structures by selective bandgap tuning," *IEEE Photon. Technol. Lett.*, vol. 3, pp. 817–820, Sept. 1991.

[7] J. H. Lee, S. K. Si, Y. B. Moon, E. J. Yoon, and S. J. Kim, "Bandgap tuning of $In_{0.53}Ga_{0.47}$ As/InP multiquantum well structure by impurity free vacancy diffusion using $In_{0.53}Ga_{0.47}$ As cap layer and SiO_2 dielectric capping," *Electron. Lett.*, vol. 33, pp. 1179–1180, 1997.

[8] S. K. Si, D. H. Yeo, K. H. Yoon, and S. J. Kim, "Area selectivity of InGaAsP–InP multiquantum-well intermixing by impurity-free vacancy diffusion," *IEEE J. Select. Topics Quantum Electron.*, vol. 4, pp. 619–623, 1998.

[9] D. H. Yeo, K. H. Yoon, and S. J. Kim, "Characteristics of intermixed InGaAs/InGaAsP multi-quantum-well structure," *Jpn. J. Appl. Phys.*, vol. 39, pp. 1032–1034, 2000.

[10] J. W. Park, H. S. Kim, J. S. Kim, D. K. Oh, K. R. Oh, D. H. Yeo, and S. J. Kim, "Intermixing characteristics of strained-InGaAs/InGaAsP multiple quantum well structure using impurity-free vacancy diffusion," *Jpn. J. Appl. Phys.*, vol. 38, pp. L1303–L1305, 1999.

[11] J. E. Zucker, B. Tell, K. L. Jones, M. D. Divino, K. F. Brown-Goebeler, C. H. Joyner, B. I. Miller, and M. G. Young, "Large blueshifting of InGaAs/InP quantum-well band gaps by ion implantation," *Appl. Phys. Lett.*, vol. 60, pp. 3036–3038, 1992.

[12] M. Razeghi, O. Acher, and F. Launay, "Disorder of a $Ga_xIn_{1-x}As_yP_{1-y}$-InP quantum well by Zn diffusion," *Semicond. Sci. Technol.*, vol. 2, pp. 793–796, 1987.

[13] K. Kato, S. Hata, K. Kawano, J. Yoshida, and A. Kozen, "A high-efficiency 50 GHz InGaAs multimode waveguide photodetector," *IEEE J. Quantum Electron.*, vol. 28, no. 12, pp. 2728–2735, 1992.

[14] K. Kato, S. Hata, A. Kozen, J.-I. Yoshida, and K. Kawano, "High-efficiency waveguide InGaAs pin photodiode with bandwidth of over 40 GHz," *IEEE Photon.Technol. Lett.*, vol. 3, pp. 473–474, 1991.

[15] W. P. Gillin, D. J. Dunstan, K. P. Homewood, L. K. Howard, and B. J. Sealy, "Interdiffusion in InGaAs/GaAs quantum well structures as a function of depth," *J. Appl. Phys.*, vol. 73, pp. 3782–3786, 1993.

[16] A. Larsson, P. A. Andrekson, S. T. Eng, and A. Yariv, "Tunable superlattice p-i-n photodetectors: Characteristics, theory, and applications," *J. Quantum Electron.*, vol. 24, pp. 787–801, May 1988.

Deok Ho Yeo was born in Yaechon, Korea, in 1971. He received the B.S. degree in physics in 1994 and the M.S. and Ph.D. degrees in electrical engineering in 1996 and 2001, respectively, from Seoul National University, Seoul, Korea.

He is with LG Elite (Electronics Institute of Technology), Seoul, Korea, where he works on the development of high-power laser diodes. His research interests include quantum-well intermixing, photonic integrated circuits, and laser diodes.

Kyung Hun Yoon was born in Cheonbook, Korea, in 1971. He received the B.S. degree in physics and the M.S. degree in electrical engineering from Seoul National University, Seoul, Korea, in 1996 and 1998, respectively. He is currently working toward the Ph.D. degree in electrical engineering.

His research interests include the design and fabrication of optoelectronic devices.

Hang Ro Kim was born in Seoul, Korea, in 1975. He received the B.S. and M.S. degrees in electrical engineering from Seoul National University, Seoul, Korea, in 1998 and 2000, respectively.

He is now with Samsung Electronics, Kyunggi-Do, Korea, and works on the design of digital circuits. His research interests include the design and fabrication of optoelectronic devices and system on a chip.

Sung June Kim (S'79–M'84) was born in Seoul, Korea, in 1954. He received the B.S. degree in electronics engineering from Seoul National University, Seoul, Korea, in 1978, and the M.S. and Ph.D. degrees from Cornell University, Ithaca, NY, in 1981 and 1983, respectively. His dissertation was on bioelectronics area.

He was with AT&T Bell Laboratories as a member of the Technical Staff from 1983 to 1989, where he worked on VLSI design and technologies, and InP-based optoelectronic IC technologies. In 1989, he joined the Interuniversity Semiconductor Research Center and the Department of Electronics Engineering, Seoul National University, where he is currently a Full Professor in the School of Electrical Engineering and Computer Science. Since August 2000, he has been the Director of Nano BioElectronics and Systems Research Center, an ERC funded by Korean Ministry of Science and Technology. His research interests are in the areas of design and fabrication of optoelectronic devices, photonic switching, neural prothesis, bioelectronics, and bioinstrumentation. He has published over 60 papers, and has managed many research projects in the areas mentioned.